Optics Letters

High-sensitivity gas pressure sensor based on a multimode interferometer using hollow-core tube lattice fiber

Zhengyong Li,[1,2] Changrui Liao,[1,2,*] Yatao Yang,[3] Ying Wang,[1,2] and Yiping Wang[1,2]

[1]Key Laboratory of Optoelectronic Devices and Systems of Ministry of Education and Guangdong Province, College of Optoelectronic Engineering, Shenzhen University, Shenzhen 518060, China
[2]Guangdong and Hong Kong Joint Research Centre for Optical Fiber Sensors, College of Physics and Optoelectronic Engineering, Shenzhen University, Shenzhen 518060, China
[3]College of Electronics and Information Engineering, Shenzhen University, Shenzhen 518060, China
*Corresponding author: cliao@szu.edu.cn

Received 4 June 2020; accepted 14 July 2020; posted 15 July 2020 (Doc. ID 399577); published 11 August 2020

A non-diaphragm fiber gas pressure sensor based on a multimode interferometer (MI) using a hollow-core tube lattice fiber (HC-TLF) as a gas cell is proposed and experimentally demonstrated. The sensor is fabricated by fusion splicing a sandwich structure of a graded-index multimode fiber, HC-TLF, and lead-in/out single mode fiber. Several side-holes are drilled by using a femtosecond laser on the side wall of the HC-TLF to allow gas in and out of the fiber. The positions of side-hole in HC-TLF have been investigated during the experiments, which indicate that the highest gas pressure sensitivity existed as the side-hole located in the gap between adjacent cladding holes of the HC-TLF. The proposed structure exhibits a high sensitivity of 8.1 nm/MPa with the average gas fill time of 2.2 s. This sensor also has low temperature sensitivity and low temperature cross sensitivity of 12.3 pm/°C and 1.5 kPa/°C as the temperature rises to 400°C. In addition, the advantages of the gas pressure sensor, such as small size, rapid response, low temperature cross sensitivity, and simple fabrication process, make it suitable for high-pressure measurement in harsh conditions, e.g., downhole and ocean bottom.

https://doi.org/10.1364/OL.399577

Fiber optical gas pressure sensors have been extensively investigated and widely used in various fields, such as meteorological monitoring, wind tunnel test, and downhole detection, due to the advantages of high sensitivity, immunity to electromagnetic interference, and remote sensing. Over the past few decades, various optic fiber gas pressure sensors such as fiber Bragg gratings (FBGs) [1], Michelson interferometers [2], Mach–Zehnder interferometers (MZIs) [3], and Fabry–Perot interferometers (FPIs) [4–6] have shown a blowout growth. Among those sensors, FPIs account for the vast majority because of the simple manufacture, high sensitivity, and reflection operation mode. A submicron diaphragm is usually applied in FPI to increase the gas pressure sensitivity. With a thickness of ~300 nm for a silver diaphragm, the FPI pressure sensor exhibited a sensitivity of 1.6 nm/kPa with the pressure range of 0–50 psi [7]. However, the diaphragm thickness restricts this type of gas pressure sensor to bear higher pressure. The diaphragm may fall off under long-term high pressure or high temperature [4]. The optical fiber gas pressure sensors based on an open cavity can overcome these issues due to the refractive index (RI) modulation of gas in the cavity. A section of hollow-core fiber (HCF) was spliced between two single mode fibers (SMFs), and a microchannel was drilled by a femtosecond (Fs) laser to open the cavity, in which the gas pressure sensitivity was obtained to be 3.592 nm/Mpa with the pressure range of 0–2 MPa [8]. However, the microchannel in the HCF can affect the light propagation along the inner wall.

Besides, various types of special optical fibers have attracted great interest for pressure application because of flexible structure designs. A dual hollow-core anti-resonant fiber with an air core air gap acts as a supermodal interferometer for gas pressure sensing with ultrahigh sensitivity of 39.3 nm/MPa [9]. A side-hole photonic crystal fiber [10] and a capillary fiber with an embedded core [11] based on the principle of pressure-induced material birefringence variation exhibits a high-pressure sensitivity of 2.22 nm/MPa and 1.04 nm/bar, respectively. Hollow-core tube lattice fibers (HC-TLFs) with the cladding consisting only of one row of silica capillaries restrict guide light propagating in the hollow core and inhibit coupling between the core and the cladding modes [12]. The large hollow core makes this fiber suitable for gas/liquid sensing, high-power lasers, and biosensors.

In this Letter, a novel multimode interferometer (MI) sensor based on HC-TLF is proposed and demonstrated for gas pressure measurement. The sensor is constructed by interposing HC-TLF between two graded-index multimode fibers (GIF) connected with SMFs. In order to open the air core of HC-TLF, an Fs laser was employed to drill side-holes on the side wall of the HC-TLF. The influence of the side-hole position for gas pressure sensitivity was investigated experimentally. The results indicate that the highest gas pressure sensitivity existed as the side-hole located in the gap between adjacent cladding holes of

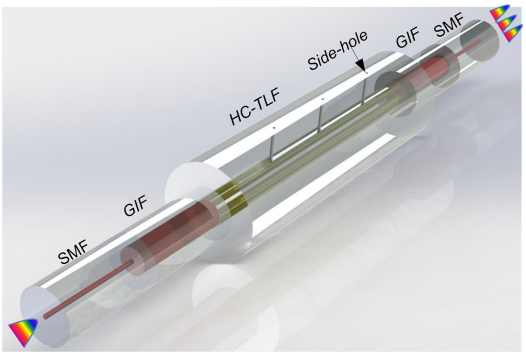

Fig. 1. Schematic diagram of the gas pressure sensor.

the HC-TLF. The samples with different HC-TLF lengths were fabricated and measured, which obtain the highest gas pressure sensitivity of 8.1 nm/MPa with an HC-TLF length of 5 cm in an average gas filled time of 2.2 s. The minimum detection limit can be calculated to be ∼2.4 KPa. In addition, a temperature response is measured and obtains a low temperature sensitivity of 12.3 pm/°C with a low temperature cross sensitivity of 1.5 kPa/°C as the temperature rises to 400°C. Hence, this gas pressure sensor with fast response, low temperature cross sensitivity, and simple fabrication has potential for high-pressure measurement in harsh conditions, e.g., downhole and ocean bottom.

The schematic diagram of the HC-TLF-based MI sensor is shown in Fig. 1. The GIF acting as a light field divergence and convergence is profitable to form a stable and large mode field in the GIF compared to the SMF. The GIF is chosen instead of the step-index multimode fiber due to the mode dispersion, and the numbers of excited guide modes are much smaller. The key component of the sensor is a segment of HC-TLF, which acts as a sensing role. As the input light is launched into GIF through the lead-in SMF, the light field can diverge to the maximum at the quarter-pitch position(245 μm) [13]. Then, the light is transmitted into the HC-TLF. A series of independent intrinsic modes are excited from the fundamental mode at the splice point owing to the mismatched mode field between GIF and HC-TLF. Because each mode has different propagation constants, interference will occur and cause redistribution of energy. Due to the characteristic designed air-hole cladding of the HC-TLF, light can be confined to travel inside the hollow core with low loss based on photonic bandgaps [14]. Finally, the light from the HC-TLF will be converged and then coupled into lead-out SMF. If the air core of the HC-TLF was exposed artificially, the light field inside the fiber will change with the external environment (temperature, pressure, RI). This could cause variation of the transmission spectrum and output light power.

According to the theory of light interference, when the phase difference between two different modes is an integer multiple of 2π, the transmitted light will coherently superimpose. The coherent condition is shown as

$$(\beta_m - \beta_n)L = 2\pi N, \tag{1}$$

where β is the propagation constant of the multimode, m and n are integer constants that delegate the mth and nth-order mode fields, L is the length of the MI sensor, and N is a constant. The wavelength of the resonant dips satisfy the condition as follows:

$$\lambda_m = \frac{2}{2m+1}\Delta n_{\text{eff}} L, \tag{2}$$

where Δn_{eff} is the effective RI difference between interferential modes, and λ_m is the central wavelength of the mth-order resonant dip. It indicates that the Δn_{eff} and L can affect the characteristic wavelength shift.

The fabrication process of the MI sensor was simply using fusion splicing technology. The microscope image of the proposed structure is shown in Fig. 2(a). First, a standard SMF [Corning, Fig. 2(b)] with core/cladding diameters of 9/125 μm was spliced with a section of GIF [YOFC, Fig. 2(c)] with core/cladding of 62.5/125 μm by means of a commercial fusion plicer (Fujikura FSM-60s). Then, the GIF was cut to the quarter-pitch position (a length of 245 μm) using a cutting system with a precision of ±5 μm. Second, this section was spliced with a HC-TLF (YSL Photonics) with hollow-core/cladding diameters of 45/245 μm. Due to the larger cladding diameter of the HC-TLF, the manual splicing procedure with lower discharge current (stander +85) and time (800 ms) was chosen during the splicing process, which can prevent the air-hole cladding from collapsing. The resulting insertion loss was determined by the quality of the spliced point. Finally, the other end of the HC-TLF was spliced with another section. To monitor the quality of the MI sensor, the samples were connected to a broadband light source (BBS) with a wavelength range from 1250 to 1650 nm (Fiber Lake ASE-LIGHT SOURCE) and an optical spectrum analyzer (OSA, YOKOGAWA AQ6370C) to measure the transmission spectra. Figure 3(a) shows the transmission spectra of the samples with/without GIF. In order to determine the number and amplitude distribution of the modes that contribute to the interferometric spectra in Fig. 3(a), fast Fourier transforms (FFT) were applied to obtain the corresponding spatial frequency spectra, as shown in the inset of

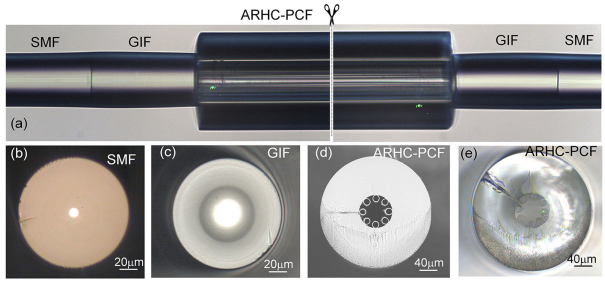

Fig. 2. (a) Microscope image of the MI sensor. The cross section of the fibers: (b) SMF, (c) GIF, (d) HC-TLF with the side-hole in cladding hole, and (e) HC-TLF with side-hole between adjacent cladding holes.

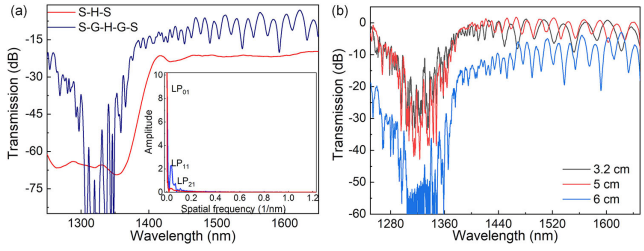

Fig. 3. (a) Transmission spectra of the structure without and with GIF. Inset: the Fourier transforms of the transmission spectra in (a). (b) Transmission spectra of the MIs with the HC-TLF lengths of 3.2, 5, and 6 cm.

Fig. 3(a). It can be found that no interference appears in the transmission spectrum (red line), as the sample is composed by a sandwich of SMF, HC-TLF, and SMF, because no high-order modes can be excited from the SMF to the HC-TLF. There are two mode interferences in the transmission spectrum (blue line) as the GIFs are inserted into the structure. According to the mode simulation results in Ref. [11], linearly polarized (LP) modes, LP_{01}, LP_{11}, and LP_{21}, can propagate in HC-TLF, and the mode loss of LP_{21} is higher than the others. Hence, the intensity of LP_{21} is much weaker than LP_{11}, which induces unapparent mode interference concealing in interference spectrum. To study the relationship between the free spectral range (FSR) and the HC-TLF length, the samples with different HC-TLF lengths (3.2 cm, 5 cm, 6 cm) have been fabricated, and the transmission spectra were measured, shown in Fig. 3(b). The results indicate that the FSR decreases with the increasing HC-TLF length.

In order to investigate the influence of high-pressure gas entering the HC-TLF, several holes were drilled in the fiber to allow high-pressure gas in and out of the HC-TLF. A Fs laser (Spectra-Physics, Solstice) with the wavelength of 800 nm, pulse duration of 120 fs, and repetition rate of 1 kHz was employed to drill holes in HC-TLF [15]. The laser power was maintained at 28 mW by an attenuator. The laser beam was focused on the surface of the HC-TLF by a 10x microscope objective (NA = 0.25) and then entered into the fiber at a speed of 0.1 μm/s. After shifting a distance of 70 μm, the side-hole was fabricated. Then, the laser beam moved to the next position and repeated the same process. Two types of side-holes were designed and fabricated. One is the side-hole located in the cladding hole, shown in Fig. 2(d). It can be seen that the hole just extended to cladding hole. The other is the side-hole located between the adjacent cladding holes, shown in Fig. 2(e). The side-holes connected to the air core of the HC-TLF and did almost no damage to the periodic structure of the cladding.

Three approaches have been designed and implemented to investigate the influence for the location of side-holes in HC-TLF. Three samples with the same HC-TLF length of 3.5 cm were sealed into the gas chamber. The gas pressure generator device was similar to Ref. [3]. The gas pressure is increased from 0 to 2.8 MPa with a step of 0.3 MPa and maintained for 5 min at each measurement point. The transmission spectra are shown in the inset of Fig. 4(a), which indicates that the fringe dips shift toward shorter wavelengths with applied pressure. Figure 4(a) shows the dip wavelength shifting trend via the gas pressure increasing. The sample without the side-hole has the gas pressure sensitivity of −0.9 nm/MPa. When the side-hole is located in the cladding hole or between adjacent cladding holes, the sensitivity was −2.3 nm/MPa and −5.6 nm/MPa, respectively. The diameter of cladding is much bigger than the core ($R_{core}/R_{cladding} = 0.16$). For the sample without side-holes, pressure-induced material birefringence in the HC-TLF is much smaller than that in Ref. [16], which acts with a slight effect on dip wavelength shift. The function of side-holes in HC-TLF is to allow the applied pressured air entering and exiting the hollow core, which can maintain the pressure balance inside and outside the fiber. It can eliminate the influence of pressure-induced material birefringence variation. In this case, pressure-induced air RI variation in the hollow core plays a leading role. This is the reason why the sensivity of the sample with side-holes is much bigger than that without side-holes.

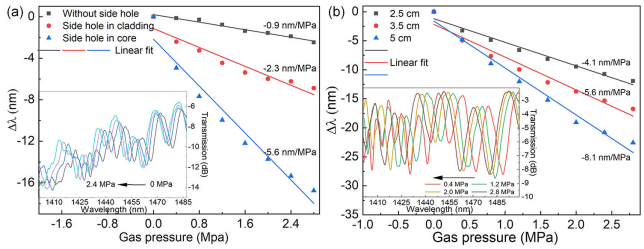

Fig. 4. Relationship between relative dip wavelength shift of the transmission spectra and gas pressure (a) with different locations of side-holes such as without a side-hole, a side-hole in the cladding, and in the core and (b) with different HC-TLF lengths of 2.5, 3.5, and 5 cm. Inset: the transmission spectra varying with applied gas pressure in (a) and (b).

According to the above conclusion, the samples with different HC-TLF lengths were fabricated and sealed into the gas chamber as the side-holes located between the adjacent cladding holes. The transmission spectra [the inset of Fig. 4(b)] are recorded by an OSA, and the variation trends via applied gas pressure are shown in Fig. 4(b). It can be found that the increase in gas pressure sensitivity is accompanied by an increase of HC-TLF lengths. The highest sensitivity is −8.1 nm/MPa with the length of 5 cm. When the OSA was working with a resolution of 0.02 nm, the minimum detectable pressure change is calculated to be ∼2.4 KPa. According to Eq. (2), the gas pressure sensitivity can be expressed as

$$\frac{\partial \lambda}{\partial P} = 2\Delta n_{\text{eff}} \frac{\partial L_G}{\partial P} + \Delta n_{\text{eff}} \frac{\partial L_H}{\partial P} + (2L_G + L_H) \frac{\partial \Delta n_{\text{eff}}}{\partial P}, \tag{3}$$

where $\partial L_G/\partial P$ and $\partial L_H/\partial P$ are the pressurized lengths coefficient of the GIF and HC-TLF, L_G and L_H are the applied lengths in MI, and $\partial \Delta n_{\text{eff}}/\partial P$ is the pressure-induced RI variation coefficient. Our previous work has demonstrated that pressure-induced fiber length variation was much smaller, which could be ignored. The pressure-induced RI variation was the leading function for the reason of wavelength shift [3]. From Eq. (3), it demonstrates a positive correlation between gas pressure sensitivity and HC-TLF length (GIF length is fixed). The experimental results shown in Fig. 4(b) also demonstrate the relationship. The performance of other pressure sensors is compared with the proposed sensor, and the data is presented in Table 1. It can be seen that the gas pressure sensor based on the side-hole HC-TLF exhibits much higher sensitivity and potential than other structures with an increase of the HC-TLF length.

Table 1. Compared with Other Gas Pressure Sensors

	Pressure (MPa)	Sensitivity (nm/MPa)
Hollow-core fiber [8]	0–2	3.592
FPI [17]	0–5	3.884
Photonic crystal fiber [10]	0–5	2.22
Photonic bandgap fiber [18]	0–0.6	−1.3
Our structure	0–2.8	−8.1

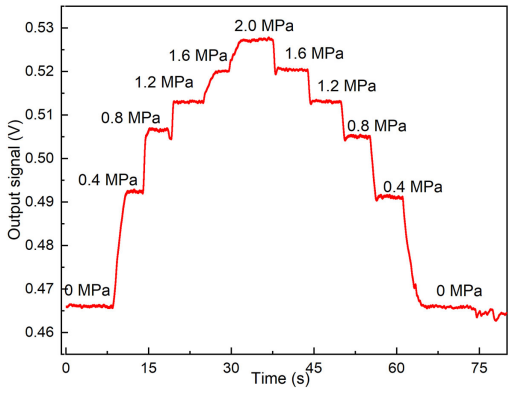

Fig. 5. Response of the proposed MI sensor during the increasing and decreasing gas pressure.

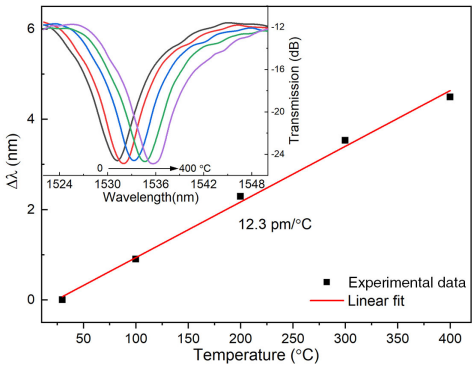

Fig. 6. Relationship between relative dip wavelength shift and temperature. Inset: the transmission spectra evaluation via the temperature increasing to 400°C.

To investigate the temporal response of the HC-TLF-based MI, the sample was connected to a tunable laser and a photoelectric detector. An oscilloscope is used to observe the variation and record the data with the applied gas pressure. The results are shown in Fig. 5, where the average response time is 2.2 s and 2.9 s as the gas pressure increases and decreases in a step, respectively. The response time is determinated by the quantity and the size of the side-hole. Moreover, it demonstrates the stability of the proposed MI sensor during the boost and buck process.

Furthermore, the temperature response of the HC-TLF-based MI sensor was investigated using a tube furnace (Carbolite, Gero HTRH). The temperature in the furnace was increased from room temperature to 400°C at a step of 100°C and maintained for 20 min at each measurement point to assure the stability of the transmission spectra. A red shift is clearly observed as the temperature increases, shown in the inset picture of Fig. 6. In addition, the relationship between relative dip wavelength shift and temperature is displayed in Fig. 6, where a good linear response with the temperature sensitivity of 12.3 pm/°C is obtained. In case no temperature compensation is employed in practical measurements, the gas pressure measurement error resulting from temperature is 1.5 kPa/°C, which is lower than the minimum detectable gas pressure change (2.4 kPa). Hence, the pressure temperature crosstalk can be ignored.

In summary, we reported an HC-TLF-based MI sensor for gas pressure measurement. The air core of the HC-TLF as a gas cell is a sensing component. The MI sensor is comprised by a sandwich structure of SMF, GIF, and HC-TLF. A Fs laser was employed to drill side-holes on the side wall of the HC-TLF, which allows high-pressure gas to enter/exit the fiber. The positions of the side-hole in the HC-TLF have been investigated during the experiments, which indicate that the highest gas pressure sensitivity existed as the side-hole located in the gap between adjacent cladding holes of the HC-TLF. The proposed MI sensor exhibits an ultrahigh gas pressure sensitivity of 8.1 nm/MPa with an average gas fill time of 2.2 s. In addition, a temperature test obtains a low temperature sensitivity of 12.3 pm/°C and low temperature cross sensitivity of 1.5 kPa/°C as the temperature rises to 400°C. Hence, such a rapid response, low temperature cross sensitivity, and simple fabrication process gas pressure sensor has potential for high-pressure measurement in harsh conditions, i.e., downhole and ocean bottom.

Funding. National Natural Science Foundation of China (61635007, 61675137, 61905162, 91860138); China Postdoctoral Science Foundation (2018M640816, 2019T120749); Natural Science Foundation of Guangdong Province (2018B030306003); Science and Technology Innovation Commission of Shenzhen (JCYJ20170818093743767).

Disclosures. The authors declare no conflicts of interest.

REFERENCES

1. P. G. Jia, G. C. Fang, T. Liang, Y. P. Hong, Q. L. Tan, X. Y. Chen, W. Y. Liu, C. Y. Xue, J. Liu, W. D. Zhang, and J. J. Xiong, Sens. Actuators B Chem. **244**, 226 (2017).
2. T. M. Zhao, J. L. Li, H. Zeng, Y. M. Fu, H. X. He, L. L. Xing, Y. Zhang, and X. Y. Xue, Nanotechnology **29**, 405504 (2018).
3. J. X. Luo, L. Shen, Y. Y. Zhao, Y. P. Chen, K. M. Yang, K. K. Guo, H. Jun, C. R. Liao, and Y. P. Wang, Opt. Lett. **45**, 507 (2019).
4. S. X. Zhang, Y. Liu, H. Y. Guo, A. Zhou, and L. B. Yuan, IEEE Sens. J. **19**, 2148 (2019).
5. F. Ahmed, V. Ahsani, K. Nazeri, E. Marzband, C. Bradley, E. Toyserkani, and M. B. G. Jun, Sensors **19**, 3357 (2019).
6. H. J. Chen, X. H. Hu, M. F. He, P. F. Ren, C. Zhang, and H. Qu, Sensors **20**, 1191 (2020).
7. L. Zhang, Y. Jiang, H. Gao, J. Jia, Y. Cui, W. Ma, S. Wang, and J. Hu, Rev. Sci. Instrum. **90**, 025005 (2019).
8. Z. Zhang, C. R. Liao, J. Tang, Z. Y. Bai, K. K. Guo, M. X. Hou, J. He, Y. Wang, S. Liu, F. Zhang, and Y. P. Wang, J. Lightwave Technol. **35**, 4067 (2017).
9. Z. Li, Y. X. Zhang, W. G. Zhang, L. X. Kong, T. Y. Yan, P. C. Geng, and B. Wang, J. Lightwave Technol. **37**, 3444 (2019).
10. F. Guo, T. Fink, M. Han, L. Koester, J. Turner, and J. S. Huang, Opt. Lett. **37**, 1505 (2012).
11. M. X. Hou, F. Zhang, Y. Wang, Y. P. Wang, C. R. Liao, S. Liu, and P. X. Lu, Opt. Express **24**, 27890 (2016).
12. F. Zhang, X. Xu, J. He, B. Du, and Y. Wang, Opt. Lett. **44**, 2466 (2019).
13. L. Vincetti and L. Rosa, Opt. Express **27**, 5230 (2019).
14. Z. Y. Li, C. R. Liao, Y. P. Wang, X. P. Dong, S. Liu, K. M. Yang, Q. Wang, and J. T. Zhou, Opt. Lett. **39**, 4982 (2014).
15. Z. Y. Li, C. R. Liao, Y. P. Wang, L. Xu, D. N. Wang, X. P. Dong, S. Liu, Q. Wang, K. M. Yang, and J. G. Zhou, Opt. Express **23**, 6673 (2015).
16. J. H. Osorio, G. Chesini, V. A. Serrao, M. A. R. Franco, and C. M. B. Cordeiro, Scientific Reports **7**, 2290 (2017).
17. H. C. Gao, Y. Jiang, L. C. Zhang, Y. Cui, Y. Jiang, J. S. Jia, and L. Jiang, Optics Express **27**, 22181 (2019).
18. J. Tang, Z. Zhang, G. L. Yin, S. Liu, Z. Y. Bai, Z. Y. Li, M. Deng, Y. Wang, C. R. Liao, J. He, W. Jin, G. D. Peng, and Y. P. Wang, IEEE Sensors Journal **9**, 7105307 (2017).